WOOD RESEARCH doi.org/10.37763/wr.1336-4561/71.2.207217
e-ISSN 2729-8906
71(2): 2026 207-217 pp.

THE COMPRESSION PARALLEL TO GRAIN STRESS-STRAIN MODEL OF TWELVE TROPICAL WOOD SPECIES WITH SPECIFIC GRAVITY RANGE OF 0.39 TO 0.67 g/cm^3

YOSAFAT AJI PRANATA[1], AMOS SETIADI[2], OLGA CATHERINA PATTIPAWAEJ[1], AAN DARMAWAN HANGKAWIDJAJA[1]
[1]UNIVERSITAS KRISTEN MARANATHA, INDONESIA
[2]UNIVERSITAS ATMA JAYA YOGYAKARTA, INDONESIA

(RECEIVED MARCH 2026)

ABSTRACT

This study aims to propose a compression parallel to grain stress-strain model equation for tropical wood species with a specific gravity range of 0.39 to 0.67 g/cm^3. The stress-strain model is compiled from the results of experimental testing of twelve tropical wood species based on empirical data of stress-strain relationship curves from destructive testing. The test uses a reference according to ASTM D143-22. The results of this study are empirical equations for calculating and creating stress-strain relationship curves in the longitudinal direction of wood (compression parallel to grain).

KEYWORDS: Compression, parallel to grain, stress-strain, tropical wood.

INTRODUCTION

Wooden buildings, especially multi-storey ones, generally use a frame structure system consisting of beams and columns (Cao et al. 2022; Premrov and Leskovar 2023). The truss-type bridge or roof truss structures consist of compression elements and tension elements (Kromoser et al. 2020; Bergenudd et al. 2024). The compressive strength parallel to the grain (longitudinal direction), is used in the design of columns in wooden frame structures and compression elements in wooden truss structures. In the analysis of nonlinear wooden building structures. For example, collapse analysis of wooden buildings (Karina et al. 2018; Cheng et al. 2021; Hua et al. 2023; Yu and Takeuchi 2024; Cao et al. 2024; Quizanga et al. 2025; Pranata 2026), a complete stress-strain model of wood is required, from elastic to post-elastic behaviour.

Predicting the compressive strength of wood can be done using several methods, including resist graph and screw withdrawal tests (Xue et al. 2019) and non-destructive testing based on wave propagation velocity (Llana et al. 2020; Cobos et al. 2022). These methods have

limitations, namely, they only obtain parameters such as elastic modulus and compressive strength. Song et al. (2007) proposed several stress–strain models for wood. In this study, the compressive stress–strain relationship for compression parallel to grain follows the Glos model (Glos 1978). The Glos stress–strain model was likewise adopted in the study conducted by Liu et al. (2022). Pranata and Suryoatmono (2013) presented the results of a study on the stress-strain model of red meranti (*Shorea spp*.). Pranata et al. (2025) continues with a study on the stress-strain model of another yellow meranti (*Shorea faguetiana*) timber. The stress model in this study can be used by practitioners and academics who require parameters of compressive strength, ultimate strength, and a stress-strain model of yellow meranti wood for the longitudinal direction. Jiang et al. (2014) studied the longitudinal compressive strength and longitudinal elastic modulus of oak wood at very low and very high temperatures, with the results being an empirical linear regression equation, which describes the relationship between temperature and compressive strength. Their study did not specifically address post-elastic conditions. Han et al. (2018) presented the results on the reliability analysis on compression strength of lumber. Lahr et al. (2020) presented a study on the compressive strength of 72 Brazilian wood species. Mankowski and Laskowska (2021) presented the results of the compressive strength parallel to grain of yellow pine. Al-Musawi et al. (2024) presented a combination of experimental tests and analytical analysis to develop the compressive response parallel and perpendicular-to-the grain of wood. Karkoodi et al. (2025) presented a study on compressive parallel to grain in timber-filled-steel tubular columns made of European beech (*Fagus sylvatica*) and birch (*Betula pendula Roth*.) timbers. Totsuka et al. (2021, 2022) and Totsuka (2025) have conducted experimental studies on the compressive strength parallel to the grain of solid and engineered wood (glulam). They discussed a complete stress-strain curve model up to failure. Zumbo et al. (2026) have conducted experimental studies on the compressive strength of six hardwood species of timber.

This study aims to propose a compression parallel to grain stress-strain model for tropical wood species with a specific gravity (G) range of 0.39 to 0.67 g/cm^3. The stress-strain model is compiled from the results of experimental testing of twelve tropical wood species based on empirical data of stress-strain relationship curves from destructive testing. The test uses a compression parallel to the timber grain according to ASTM D143-22.

MATERIAL AND METHODS

Experimental tests

ASTM D143-22 provides methods for a clear specimen for testing the compression parallel to the timber grain. The specimen 50 x 50 x 200 mm were placed vertically (parallel to the grain) and loaded axially (compression) at a rate of speed of 0.305 mm/min (Hung Ta 2008), until failure to determine maximum crushing strength. Tests were conducted in air-dry conditions where the moisture content of the wood reaches 12% - 18%.

Linear regression analysis

Linear regression is a statistical method used to predict a continuous, dependent variable based on one independent variable (Starbuck 2023):

$$y = a.x + b \quad (1)$$

Methods

This research used an experimental laboratory method to obtain data on the relationship curves of axial load and axial compressive deformation in wood. ASTM D143-22 was used as a reference for compressive testing parallel to the grain. The empirical data were then processed into a relationship curve of axial stress and axial compressive strain. Stress is the load divided by the specimen's area of cross-sectional, while strain is the shortening of the specimen due to the compressive load divided by its initial length (Hibbeler 2023). The method used to determine the point of transition from elastic to plastic to calculate the yield limit load in this study was based on the EC for standardization method (Munoz et al. 2008; Liu et al. 2020). The empirical equation was constructed using a linear regression equation with input data: the correlation between wood specific gravity and yield limit load, the correlation between wood specific gravity and ultimate limit load, and the correlation between wood specific gravity and load when the material collapses.

RESULTS AND DISCUSSION

This research used data from twelve tropical timber species from Indonesia (Tab. 1, Fig. 1a). All specimens were made from dry wood raw materials with moisture content ranging from 12% to 18% (SNI 7973: 2013, NDS 2024). Compression testing uses an instrument with a load speed adjusted to the ASTM D143-22 (Fig. 1b).

Tab. 1: Specification and species of timber that used in research.

No	Species	Dimensions of specimens	Number of specimens
1	Red meranti (*Shorea parvifolia*.)	50 mm x 50 mm x 200 mm	5
2	White meranti (*Shorea montigena*)		5
3	Padi meranti (*Shorea venulosa*)		5
4	Akasia mangium (*acacia mangium*)		4
5	Gunung (*Dipterocarpus retusus*)		5
6	Yellow meranti (*Shorea faguetiana*)		4
7	Meranti bunga (*Shorea leprosula Miq*)		4
8	Kamper sumatra (*Dryobalanops aromatica*)		5
9	Meranti (*Shorea macrobalanos*)		4
10	Keruing (*Dipterocarpus*)		4
11	Kamper (*Cinnamomum camphora*)		4
12	Kamper samarinda (*Cinnamomum camphora*)		5

Fig. 1: a) Twelve tropical species of timber used in the research, b) compression test parallel to the grain according to ASTM D143-22.

For the test load a cell was installed with a capacity of up to 1000 kN, axial deformation is recorded through an internal transducer installed. Fig. 2 displays load-deformation relationship curves for specimens of all wood species. The determination of the yield limit load (P_y) parameter was calculated using the CEN method (Munoz et al. 2008; Liu et al. 2020). The ultimate limit load (P_u) was determined from the maximum load before the specimen experienced a decrease in strength after reaching the peak limit. Furthermore, the post-ultimate load (P_o) was determined from the load condition that experienced a significant decrease in strength just before the specimen lost its ability to withstand axial compressive loads.

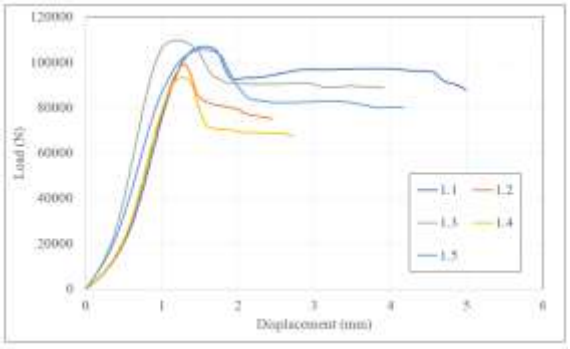

(a)

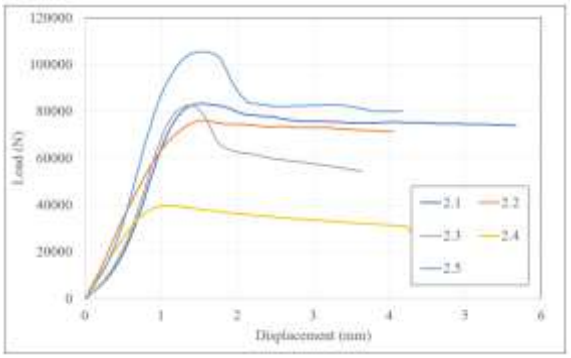

(b)

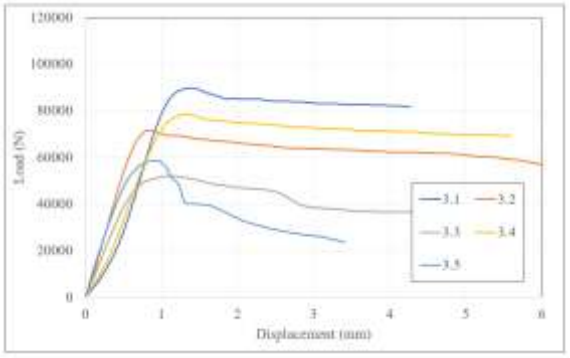

(c)

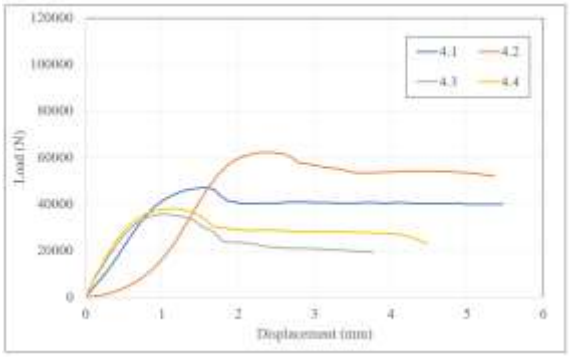

(d)

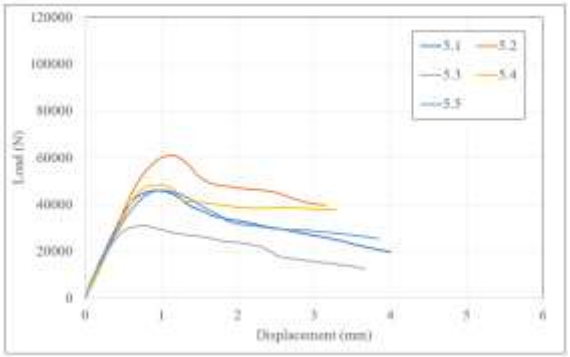

(e)

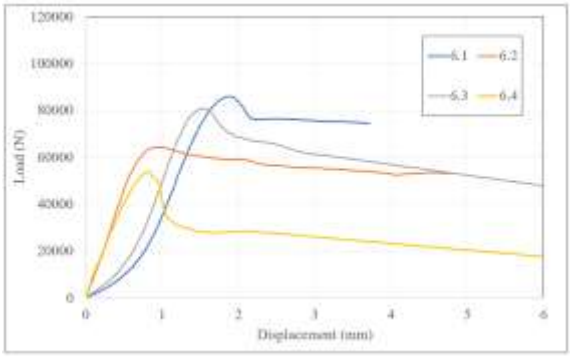

(f)

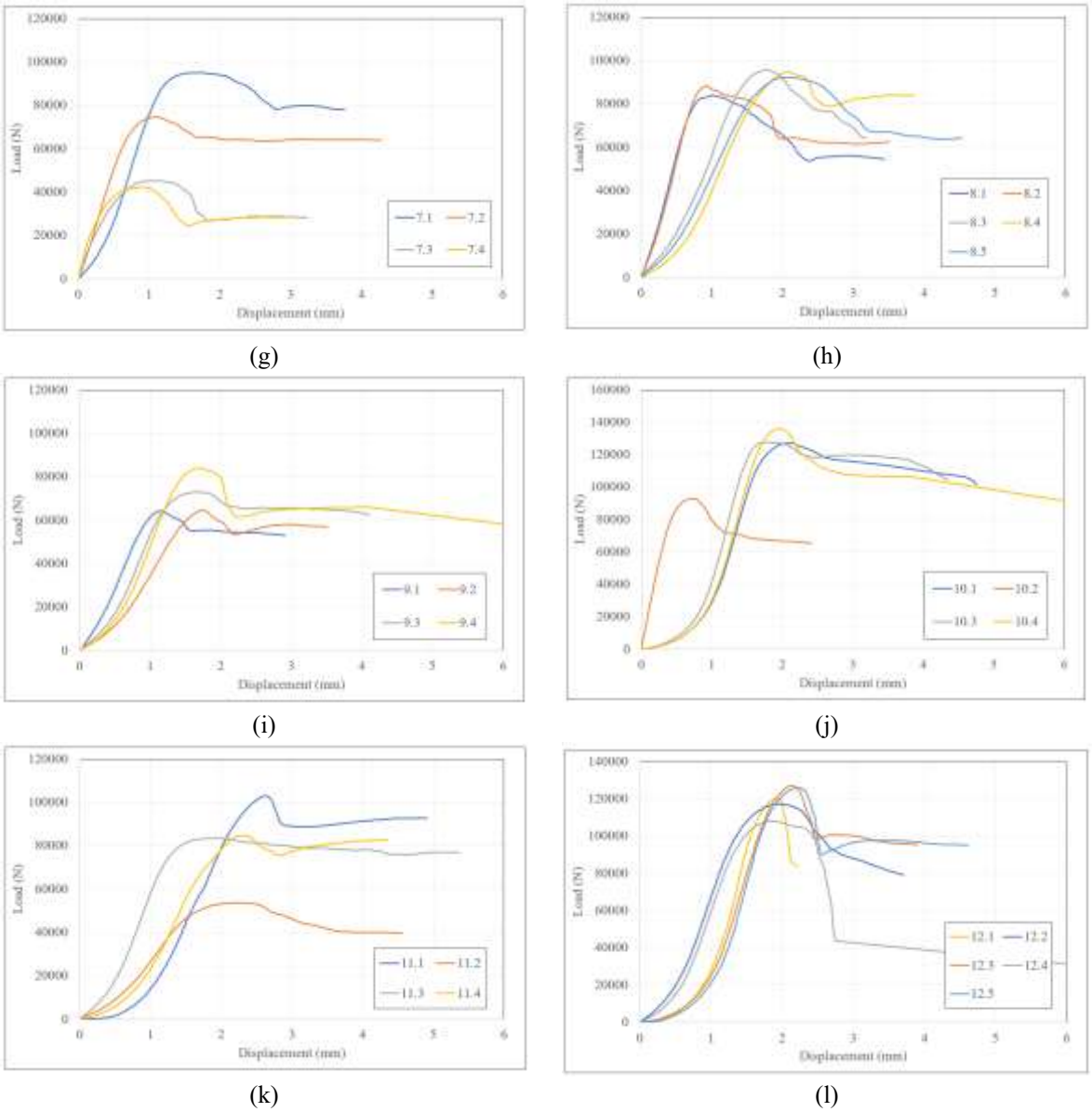

Fig. 2: The load-deformation relationship curves for: (a) Shorea *parvifolia, (b) Shorea montigena, (c) Shorea venulosa, (d) Acacia mangium, (e) Dipterocarpus retusus, (f) Shorea faguetiana, (g) Shorea leprosula Miq, (h) Dryobalanops aromatica, (i) Shorea macrobalanos, (j) Dipterocarpus, (k) Cinnamomum camphora, and (l) Cinnamomum camphora.*

The results of the yield limit load, ultimate load, and post-plastic load calculations, with deformation at each condition, are presented in Tab. 2. All parameters in Tab. 2 are average values for the specimens of each wood species. Tab. 3 shows the results in term of uniaxial stress and strain. The results generally show a general pattern, with a correlation: higher specific gravity leads to higher compressive capacity. The ductility ratio calculation (the ratio of deformation at the ultimate condition divided by deformation at the yield condition) indicates that all species fall into the limited ductility category.

Tab. 2: Load and deformation.

No	Species	G (g/cm^3)	P_y (kN)	D_y (mm)	P_u (kN)	D_u (mm)	P_o (kN)	D_o (mm)	μ
1	Red meranti (*Shorea parvifolia*.)	0.51	93.63	1.09	101.69	1.40	86.42	1.74	1.29
2	White meranti (*Shorea montigena*)	0.43	66.61	1.01	77.04	1.46	66.66	2.11	1.44
3	Padi meranti (*Shorea venulosa*)	0.39	60.81	0.74	56.30	1.18	63.71	1.61	1.59
4	Akasia mangium (*acacia mangium*)	0.42	38.76	0.98	45.27	1.57	38.92	2.09	1.61
5	Gunung (*Dipterocarpus retusus*)	0.41	40.11	0.62	45.90	0.94	39.63	1.43	1.51
6	Yellow meranti (*Shorea faguetiana*)	0.44	62.61	1.03	70.84	1.34	58.84	1.71	1.30
7	Meranti bunga (*Shorea leprosula Miq*)	0.54	56.31	0.72	64.15	1.14	49.87	1.93	1.58
8	Kamper sumatra (*Dryobalanops aromatica*)	0.51	78.88	1.17	90.77	1.60	75.32	2.31	1.36
9	Meranti (*Shorea macrobalanos*)	0.46	60.19	1.17	70.95	1.58	59.14	2.05	1.36
10	Keruing (*Dipterocarpus*)	0.67	101.77	1.25	119.93	1.62	105.50	2.20	1.29
11	Kamper (*Cinnamomum camphora*)	0.59	67.81	1.61	80.49	2.23	72.08	2.87	1.39
12	Kamper samarinda (*Cinnamomum camphora*)	0.63	103.45	1.57	116.69	2.07	94.32	2.51	1.32

Note: P_y is the yield load, P_u is the maximum (ultimate) load, P_o is the post-ultimate load, D_y is the displacement at yield point, D_u is the displacement at ultimate point, D_o is the displacement at post-ultimate point, μ is ratio of ductility (D_y divided by D_u).

Tab. 3: Stress and strain.

No	Species	F_{cy} (MPa)	ε_{cy} (mm/mm)	F_{cy} (MPa)	ε_{cy} (mm/mm)	F_{cy} (MPa)	ε_{cy} (mm/mm)
1	Red meranti (*Shorea parvifolia*.)	37.45	0.0054	40.67	0.0070	34.57	0.0087
2	White meranti (*Shorea montigena*)	26.64	0.0051	30.81	0.0073	26.66	0.0106
3	Padi meranti (*Shorea venulosa*)	24.33	0.0037	22.52	0.0059	25.48	0.0081
4	Akasia mangium (*acacia mangium*)	15.50	0.0049	18.11	0.0079	15.57	0.0104
5	Gunung (*Dipterocarpus retusus*)	16.04	0.0031	18.36	0.0047	15.85	0.0072
6	Yellow meranti (*Shorea faguetiana*)	25.05	0.0052	28.33	0.0067	23.54	0.0086
7	Meranti bunga (*Shorea leprosula Miq*)	22.52	0.0036	25.66	0.0057	19.95	0.0096
8	Kamper sumatra (*Dryobalanops aromatica*)	31.55	0.0059	36.31	0.0080	30.13	0.0115
9	Meranti (*Shorea macrobalanos*)	24.08	0.0058	28.38	0.0079	23.65	0.0102
10	Keruing (*Dipterocarpus*)	40.71	0.0063	47.97	0.0081	42.20	0.0110
11	Kamper (*Cinnamomum camphora*)	27.12	0.0080	32.20	0.0112	28.83	0.0143
12	Kamper samarinda (*Cinnamomum camphora*)	41.38	0.0079	46.68	0.0104	37.73	0.0125

Note: F_{cy} is the yield stress, F_{cu} is the ultimate stress, F_{co} is the post-ultimate stress, ε_{cy} is the yield strain, ε_{cu} is the ultimate strain, ε_{co} is the post-ultimate strain.

A linear regression analysis was performed using Minitab 2023 to obtain the correlation between the specific gravity (G) with F_{cy}, G with F_{cu}, G with F_{co}, G with ε_{cy}, G with ε_{cu}, and G with ε_{co}. The results of the regression analysis are shown in Eqs. 2 to 7, Figs. 3 to 5, and Fig. 6.

$$F_{cy} = -9.593 + 75.28\,G \quad (R^2 = 0.46 \text{ and p-value} = 0.00) \quad (2)$$

$$\varepsilon_{cy} = -0.000705 + 0.01221\,G \quad (R^2 = 0.24 \text{ and p-value} = 0.00) \quad (3)$$

$$F_{cu} = -14.49 + 92.26\,G \quad (R^2 = 0.50 \text{ and p-value} = 0.00) \quad (4)$$

$$\varepsilon_{cu} = -0.000781 + 0.01352\,G \quad (R^2 = 0.23 \text{ and p-value} = 0.00) \quad (5)$$

$$F_{co} = -8.158 + 70.91\,G \quad (R^2 = 0.42 \text{ and p-value} = 0.00) \quad (6)$$

$$\varepsilon_{co} = -0.002965 + 0.01447\,G \quad (R^2 = 0.23 \text{ and p-value} = 0.00) \quad (7)$$

Eqs. 2 to 7 exhibit relatively low coefficients of determination ($R^2 < 0.60$), the consistently low p-values (≤ 0.005) indicate that the predictor variables significantly influence compression mechanical properties of wood across yield, ultimate, and post-ultimate conditions. The limited explanatory power is likely due to inherent variability in wood specimens under field conditions, such as differences in moisture content, temperature, and tree age, which are not fully captured in the models. Nevertheless, the equations remain valuable for identifying statistically significant trends and relationships.

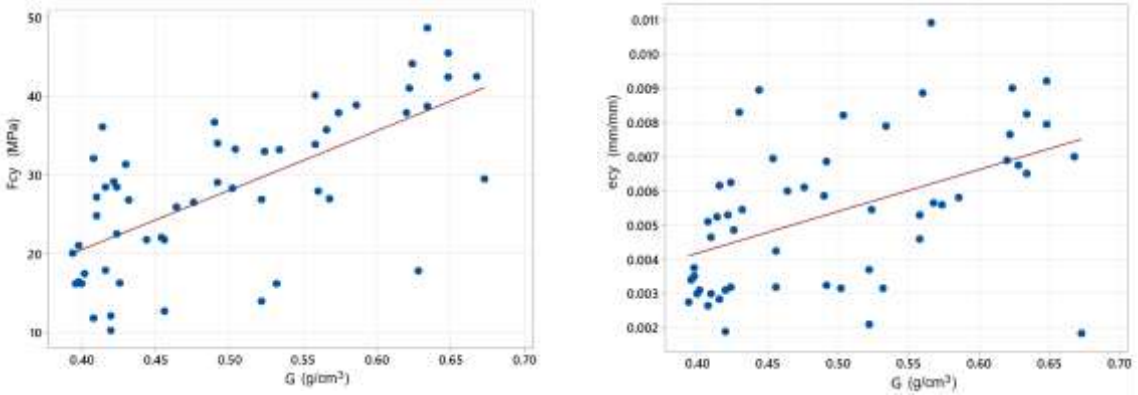

(a) (b)

Fig. 3: Results of regression analysis (a) analysis of F_{cy} and (b) analysis of ε_{cy}.

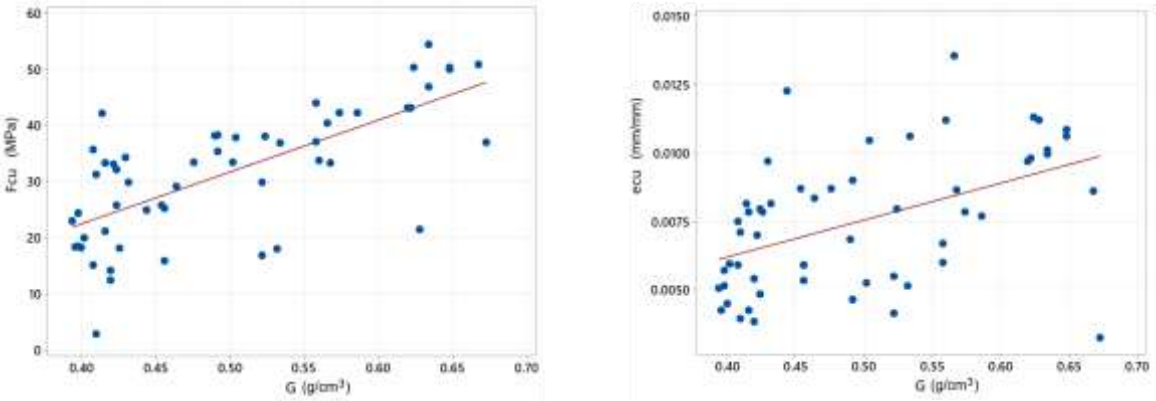

(a) (b)

Fig. 4: Results of regression analysis (a) analysis of F_{cu} and (b) analysis of ε_{cu}.

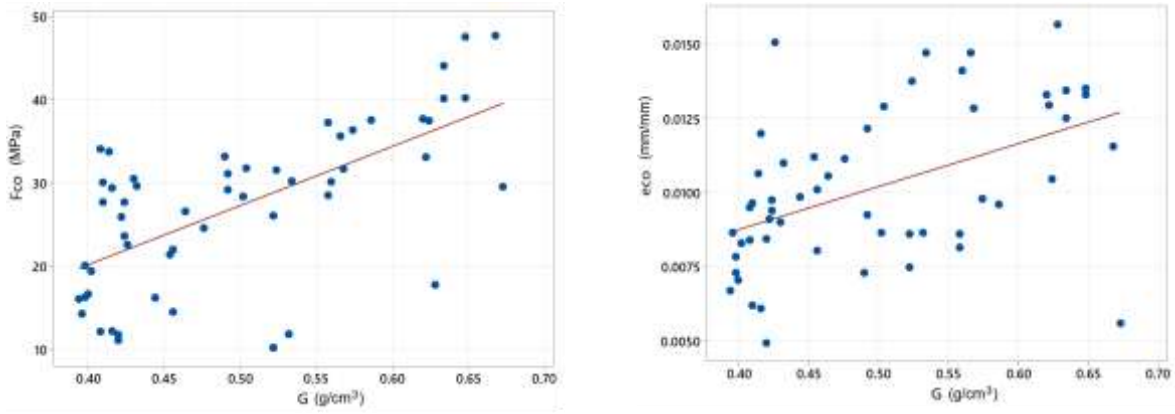

(a) (b)

Fig. 5: Results of regression analysis (a) analysis of F_{co} and (b) analysis of ε_{co}.

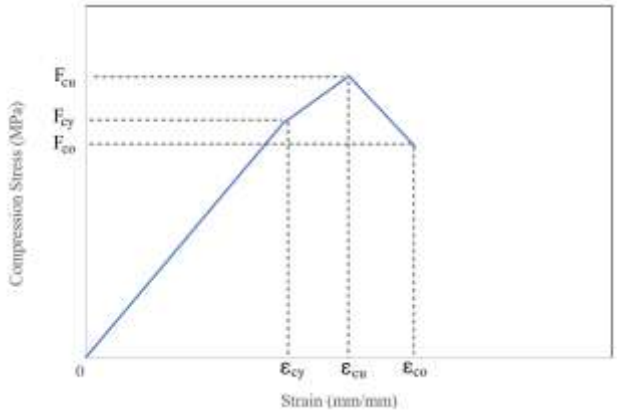

Fig. 6: Proposed compression parallel to grain stress-strain model of tropical wood species with specific gravity (G) range of 0.39 to 0.67 g/cm^3.

The stress–strain model for tropical wood derived in this study demonstrates a similar behavioural trend to the Glos model (Glos 1978; Arriaga et al. 2023), suggesting that the proposed formulation aligns well with established predictive approaches. Post-elastic and post-ultimate models are necessary for practitioners and academics when designing wooden building structures to enable analysis of building behaviour in the post-elastic range under applied external loads.

CONCLUSIONS

The results of this study are empirical equations for calculating and creating stress-strain relationship curves in the longitudinal direction of wood. Flexural strength is commonly represented by F_{cy} = -9.593 + 75.28G (R^2=0.46 and p-values 0.00), whereas the modulus of rupture is represented by F_{cu} = -14.49 + 92.26G (R^2=0.50 and p-values 0.00). Very small p-values (≤0.005) indicate that the relationships between the predictors and the response are statistically significant.

When designing beams or other flexible components for wooden constructions or bridges, these two equations are utilized. The proposed stress–strain model for longitudinal direction of wood (compression parallel to grain) developed in this study enables the estimation of the longitudinal compressive strength of wood at different stages of loading, including the yield limit, the ultimate limit (post-elastic), and the post-ultimate behaviour.

ACKNOWLEDGMENTS

The authors would like to thank Kementerian Pendidikan Tinggi, Sains, dan Teknologi Republik Indonesia for funding this research through the Penelitian Kompetitif Nasional Grant (Penelitian Fundamental Reguler) under Main Contract Number 125/C3/DT.05.00/PL/2025.

REFERENCES

1. AL-MUSAWI, H., MATZ, P., JAKOB, M., HALBAUER, P., KRENKE, T., & MULLER, U. (2024): Stress–strain behaviour of wood in compression: Experimental and analytical investigations. In: Results in Engineering, 24, 103616 pp.
2. ARRIAGA, F., WANG, X., ÍÑIGUEZ-GONZÁLEZ, G., LLANA, D.F., ESTEBAN, M., & NIEMZ, P. (2023). Mechanical properties of wood: a review. In: Forests, 14, 1202.
3. ASTM D143-22 Standard test methods for small clear specimens of timber.
4. AMERICAN WOOD COUNCIL, 2024: The 2024 National Design Specification (NDS) for wood construction. Wood Design Standards Committee.
5. BERGENUDD, J., BATTINI, J.M., & CROCETTI, R. (2024): Dynamic analysis of a pedestrian timber truss bridge at three construction stages. In: Structures, 59(2024), 105763.
6. CAO, A.S., ESSER, L., & FRANGI, A. (2024): Modelling progressive collapse of timber buildings. In; Structures, 62(2024), 106279.
7. CAO, J., XIONG, H., & CUI, Y. (2022): Seismic performance analysis of timber frames based on a calibrated simplified model. In: Journal of Building Engineering, 46(2022), 103701.
8. CHENG, X., GILBERT, B.P., GUAN, H., UNDERHILL, I.D., & KARAMPOUR, H. (2021): Experimental dynamic collapse response of post-and-beam mass timber frames under a sudden column removal scenario. In: Engineering Structures, 233(2021), 111918.
9. COBOS, G.H.V., OLVERA-LICONA, G., HERMOSO, E., & ESTEBAN, M. (2022): Nondestructive techniques for determination of wood mechanical properties of urban trees in Madrid. In: Forests 13(9), 1381.
10. CONCEPT BOIS TECHNOLOGIE. (2024). Nondestructive technology using ultrasounds for wood quality assessment. Concept Bois Technologie.
11. GLOS, P. (1978). To determine the strength behavior of glued laminated timber under compressive stress from material and load parameters (in German). Dissertation. Technische Universität München.
12. HAN, L., ZHAO, X., ZHOU, H., & LUO, X. (2018): Reliability analysis on compression strength property of chinese larch visually-graded dimension lumber. In: Wood Research, 64(3), 471-482 pp.
13. HIBBELER, R.C. (2023). Mechanics of materials. 11th edition, Pearson.
14. HUA, Y., CHUN, Q., MI, Z., & WU, Y. (2023): Experimental research on progressive collapse behavior of Chinese ancient timber buildings with different joint strengthening methods. In: Journal of Building Engineering, 68(2023), 106215.
15. HUNG TA, Co., Ltd. (2008). HT-9501 Electro-hydraulic servo universal testing machines. Hung Ta Instrument Co. Ltd.
16. JIANG, J., LU, J., ZHOU, Y., ZHAO, Y., & ZHAO, L. (2014): Compression strength and modulus of elasticity parallel to the grain of oak wood at ultra-low and high temperatures. In: BioResources, 9(2), 3571-3579 pp.

17. KARINA, C.N.N., AWALUDIN, A., SUHENDRO, B., & CHUN, P. (2018): Collapse simulation of Ammu Hawu traditional timber house in Nusa Tenggara Timur, Indonesia. In: International Journal of Technology, 9(3), 513-525 pp.
18. KARKOODI, S., KARAMPOUR, H., GILBERT, B.P., & GUNALAN, S. (2025): A study on enhanced mechanical properties of wood in the parallel-to-grain direction in timber-filled-steel tubular columns. In: Engineering Structures, 331, 119973.
19. KROMOSER, B., RITT, M., SPITZER, A., STANGI, R., & IDAM, F. (2020): Design concept for a greened timber truss bridge in city area. In: Sustainability, 12(8), 3218.
20. LAHR, F.A.R., CHAHUD, E., ARROYO, F.N., CHRISTOFORO, A.L., RODRIGUES, E.F.C., ALMEIDA, J.P.B., AQUINO, V.B.D.M., & SANTOS, H.F.D. (2020): Ratio analysis between compression and shearing of 72 Brazilian wood species. In: Wood Research, 66(5), 711-720 pp.
21. LIU, C., FERCHE, A.C., VECCHIO, F.J. (2022). Modelling short-term monotonic response of timber–concrete composite structures. Canadian Journal of Civil Engineering, 49(2), 201-211 pp.
22. LIU, Y., WANG, Y., ZHANG, Y., CHEN, M., NIE, X. (2020): Force–displacement relations of bolted timber joints with slotted-in steel plates parallel to the grain. In: Journal of Wood Science, 66:83, 1-13 pp.
23. LLANA, D.F., SHORT, I., & HARTE, A.M. (2020): Use of non-destructive test methods on Irish hardwood standing trees and small-diameter round timber for prediction of mechanical properties. In: Annals of Forest Science, 77: 62.
24. MANKOWSKI, P. & LASKOWSKA, A. (2021): Compressive strength parallel to grain of earlywood and latewood of yellow pine. Maderas. Ciencia y Tecnología, 23:57, 1-12 pp.
25. MUNOZ, W., MOHAMMAD, M., SELENIKOVICH, A. & QUENNEVILLE, P. (2008): Determination of yield point and ductility of timber assemblies: in search of harmonised approach. In; Proceeding of 10th World Conference on Timber Engineering 2008, 1064-1071 pp.
26. PRANATA, Y.A. (2026): Evaluation of ductility capacity of the two existing joglo timber buildings. In: Journal of Rehabilitation in Civil Engineering, 14(2), 2317.
27. PRANATA, Y.A. & SURYOATMONO, B. (2013): Nonlinear finite element modeling of red meranti compression at an angle to the grain. In: Journal of Engineering and Technological Science, 45 (3), 222-240 pp.
28. PRANATA, Y.A., WONG, H., NOVI, & NAIBAHO, N.A.S. (2025): Compression strength parallel to the grain of yellow meranti (*Shorea faguetiana*) Timber. In: Lecture Notes in Civil Engineering, 714, 369-376 pp.
29. PREMROV, M. & LESKOVAR, V.Z. (2023): Innovative structural systems for timber buildings: a comprehensive review of contemporary solutions. In: Buildings, 13(7), 1820.
30. QUIZANGA, D., ALMAZAN, J.L., & RODAS, P.T. (2025): Seismic Collapse of Frictionally Isolated Timber Buildings in Subduction Zones: An Assessment Considering Slider Impact. In: Buildings, 15(19), 3593.
31. SNI 7973. 2013: Design specifications for wood construction.
32. SONG, J.K., KIM, S.Y., & OH, S.W. 2007: The compressive stress-strain relationship of timber. In: Advanced Materials Research, 133-134, 1207-1211 pp.

33. STARBUCK, C. 2023: The fundamentals of people analytics. Springer Nature Link, 181-206 pp.
34. TOTSUKA, M. (2025): Evaluation method of compression parallel to grain stiffness in wood and relationship between stiffness and shape of contact surface. In: European Journal of Wood and Wood Products 83 (1), 1-15 pp.
35. TOTSUKA, M., JOCKWER, R., AOKI, K., & INAYAMA, M. (2021): Experimental study on partial compression parallel to grain of solid timber. In: Journal of Wood Science, 67:39, 1-11 pp.
36. TOTSUKA, M., JOCKWER, R., KAWAHARA, H., AOKI, K., & INAYAMA, M. (2022): Experimental study of compressive properties parallel to grain of glulam. In: Journal of Wood Science, 68 (1), 1-14 pp.
37. XUE, S., ZHOU, H., LIU, X., & WANG, W. (2019): Prediction of compression strength of wood usually used in ancient timber buildings by using resistograph and screw withdrawal tests. In: Wood Research, 64 (2), 249-260 pp.
38. YU, Y. & TAKEUCHI, W. (2024): Analysis of scattering mechanisms in SAR image simulations of Japanese wooden buildings damaged by earthquake. In: Buildings, 14, 3585 pp.
39. ZUMBO, A., MONACO, A.L., PAPANDREA, S.F., PICCHIO, R., & PROTO, A.R. (2026): Technological properties of some non-native hardwood in Mediterranean Area. In: Forests, 17(4), 444.

YOSAFAT AJI PRANATA*
UNIVERSITAS KRISTEN MARANATHA
FACULTY OF SMART TECHNOLOGY AND ENGINEERING
JL. SURIA SUMANTRI 65, BANDUNG, 40164, WEST JAVA, INDONESIA
*Corresponding author: yosafat.ap@gmail.com

AMOS SETIADI
UNIVERSITAS ATMA JAYA YOGYAKARTA
FACULTY OF ENGINEERING
JL. BABARSARI 44, SLEMAN, 55281, D.I. YOGYAKARTA, INDONESIA

OLGA CATHERINA PATTIPAWAEJ
UNIVERSITAS KRISTEN MARANATHA
FACULTY OF SMART TECHNOLOGY AND ENGINEERING
JL. SURIA SUMANTRI 65, BANDUNG, 40164, WEST JAVA, INDONESIA

AAN DARMAWAN HANGKAWIDJAJA
UNIVERSITAS KRISTEN MARANATHA
FACULTY OF SMART TECHNOLOGY AND ENGINEERING
JL. SURIA SUMANTRI 65, BANDUNG, 40164, WEST JAVA, INDONESIA